Journal of Computational and Applied Mathematics 409 (2022) 114150

Contents lists available at ScienceDirect

Journal of Computational and Applied Mathematics

journal homepage: www.elsevier.com/locate/cam

Similarity classes generated by the 8T-LE partition applied to trirectangular tetrahedra☆

Miguel A. Padrón *, Ángel Plaza

Institute for Applied Microelectronics (IUMA), Division of Mathematics, Graphics and Computing (MAGiC), University of Las Palmas de Gran Canaria (ULPGC), Campus de Tafira Baja s/n, 35017, Las Palmas de G.C., Spain

ARTICLE INFO

Article history:
Received 11 February 2021
Received in revised form 14 December 2021

Keywords:
8-tetrahedra longest-edge partition
Trirectangular tetrahedron
Similarity classes

ABSTRACT

When the 8T-LE partition is recursively applied to any initial trirectangular tetrahedron T, only a finite number of dissimilar tetrahedra are generated. It implies the *stability* of the meshes. At each step of refinement the number of *right-type* or *path* tetrahedra grows, so the quality of the obtained meshes improves. The minimum angle condition and the maximum angle condition are trivially satisfied, since the number of similarity classes is finite.

1. Introduction

We focus in this paper on the 8T-LE partition applied to a special class of tetrahedron, the *trirectangular*, *corner* or *cube* tetrahedron. This partition is the natural extension to 3D of the well-known 4 Triangles Longest-Edge partition (4T-LE) introduced and developed by Rivara [1]. Some of the suitable properties of the 4T-LE partition are the self-improvement of the mesh, the non-degeneracy and the locality of the refinement [1,2].

The regular trirectangular tetrahedron appears in five of the six triangulations of a 3D-cube, except for the Freudenthal partition. For this reason, this tetrahedron is a *binary* tetrahedron, together with the regular *right-type* tetrahedron and the *quasi right-type* tetrahedron [3–5]. The vertices of these tetrahedra are directly related with 0-1 matrices, which appear in many scenarios as graph theory or coding theory among others [6]. Also, the scalene trirectangular tetrahedron appears in five of the six triangulations of any hexahedron, except for the Freudenthal partition of the hexahedron into six scalene *right-type* tetrahedra.

Trirectangular tetrahedron also appears when a 3D-cube is subdivided into 24 isosceles trirectangular tetrahedra. A 3D-cube can be partitioned into 6 pyramids whose common vertex is at the center of gravity of the cube. Then each pyramid can be partitioned into 4 cube-corner tetrahedra see Fig. 6. This partition is called Face Centered division (FC) of a 3D-cube [7]. The triangulation of the 3D-cube following different strategies, is of interest because, the conversion from an octree-based hexahedral mesh [8] to a tetrahedral mesh is straightforward [9].

We will prove here that, for any initial trirectangular tetrahedron T, the iterative 8T-LE partition of T yields a sequence of tetrahedra where the number of classes of similarity is bounded, and hence the non-degeneracy or stability of the tetrahedral meshes follows. In the finite element method, non-degeneracy plays a very significant role for the stiffness matrix conditioning where a partial differential equation is converted into a large sparse linear system of algebraic equations to be solved. In this context, dihedral angles near 0 or near π radians, can cause large matrix entries which lead to poor matrix conditioning.

☆ This work has been supported in part by the Cabildo de Gran Canaria, Spain Project number 2018-01.
* Corresponding author.
E-mail addresses: miguel.padron@ulpgc.es (M.A. Padrón), angel.plaza@ulpgc.es (Á. Plaza).

https://doi.org/10.1016/j.cam.2022.114150

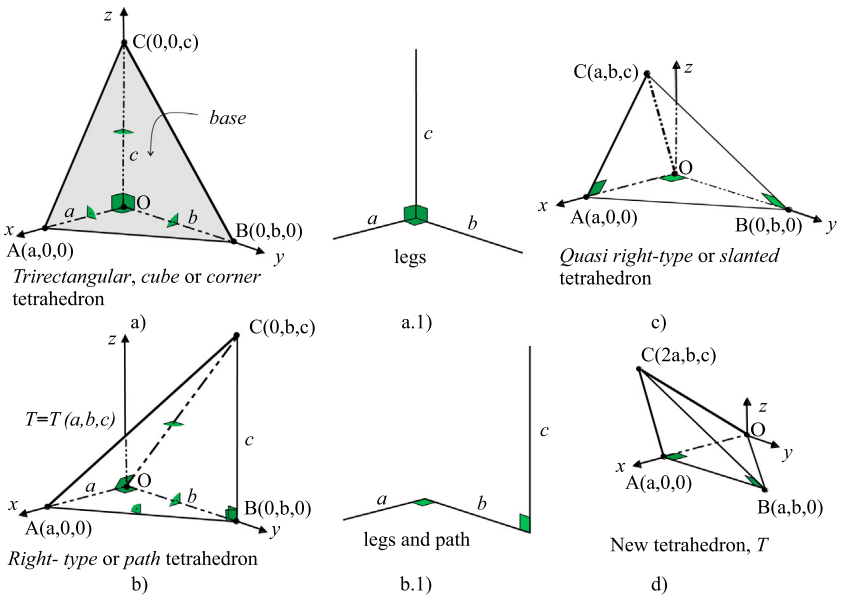

Fig. 1. Four classes of tetrahedra where $c > b > a$. Tetrahedra (a) and (b) are ortho-simplices and nonobtuse. Tetrahedra (c) and (d) are obtuse.

The number of similarity classes also directly affects the total computational work, since there are data which can be computed and stored only once per element of a given class [10], reducing hugely the computational cost, and hence improves the efficiency of the algorithms [11]. These properties, are highly desirable in many areas of engineering, such as, the finite element method.

2. Basic definitions and preliminaries

A closed subset $T \subset \mathbb{R}^n$ is called a *k-simplex*, $0 \leq k \leq n$, if T is the convex linear hull of $k+1$ affinely independent vertices $x^{(0)}, \ldots, x^{(k)} \in \mathbb{R}^n$, with T denoted by its vertices $[x^{(0)}, \ldots, x^{(k)}]$. If $k = n$ then T is simply called a *simplex* of $\mathbb{R}^n$. If $k = 2, 3$ *simplices* are called *triangles* and *tetrahedra* as usual.

For any tetrahedron T each one of the six angles between any pair of its faces is called a *dihedral interior* angle or an *interior* angle. An angle is *acute* if it is less than a right angle. A simplex is *nonobtuse* if its dihedral angles are either acute or right.

Theorem 1. *If $n > 2$ then each facet of an acute n-simplex is an acute $(n-1)$-simplex [12].*

The converse implication does not hold –see previous reference–, as it happens with the quasi right or slanted tetrahedron, as we will show later on.

Definition 1 (*Ortho-simplex and Path-simplex*)**.** In $\mathbb{R}^n$, an *ortho-simplex* is a simplex having n mutually orthogonal edges (*legs*), see Figs. 1(a) and 1(b) for the $\mathbb{R}^3$ case. An ortho-simplex can also be classified as *regular*, *isosceles* or *scalene*, depending on the legs's length. In $\mathbb{R}^n$, a *path-simplex* is an ortho-simplex whose n orthogonal edges form a path in the sense of graph theory, that is, a sequence of n edges which joins a sequence of vertices [12], see Fig. 1(b) for the $\mathbb{R}^3$ case.

Notice that each ortho-simplex is nonobtuse.

Theorem 2. *Each d-simplex has at least d acute dihedral angles. Each ortho-simplex has exactly d acute dihedral angles [12].*

Fig. 1 shows two classes of ortho-simplices in $\mathbb{R}^3$. The tetrahedron in Fig. 1(b) has only right triangular faces. It is a *path* or *right-type* tetrahedron, because its three orthogonal edges (*legs*) form a path. The tetrahedron in Fig. 1(a), has three mutually orthogonal edges (*legs*) that share a common vertex O, where all three face angles at the same vertex are right angles. That vertex is called *spatial right angle* and the face opposite it is called the *base*. All these features define a *trirectangular*, *cube* or *corner* tetrahedron. It is clear that the longest-edges of an ortho-tetrahedron are hypotenuses of its right-angled faces, and the shortest ones are the *legs*.

The right-type tetrahedron has been studied in [4], where the next theorem is stated:

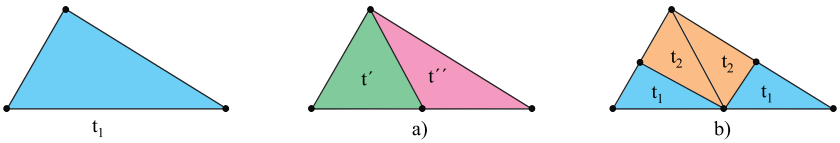

Fig. 2. (a) LE partition of triangle t_1, (b) 4T-LE partition of triangle t_1.

Theorem 3. *Two right-type tetrahedra $T_1(a_1, b_1, c_1)$ and $T_2(a_2, b_2, c_2)$ are similar if and only if their extreme legs are in the same ratio as their central legs. That is, either $\frac{b_1}{b_2} = \frac{a_1}{a_2} = \frac{c_1}{c_2}$, or $\frac{b_1}{b_2} = \frac{a_1}{c_2} = \frac{c_1}{a_2}$ [4].*

It is proved in [4] that, when the 8T-LE partition is applied to any initial right-type tetrahedron, the number of similarity classes is bounded. Also, for the regular right-type tetrahedron, all the descendants are similar (up to mirror imaging) to the original one.

Fig. 1(c) and (d) shows two classes of tetrahedra. Both tetrahedra are obtuse, although the first one its four triangular faces are not of obtuse type, see Theorem 1.

Definition 2 (*Quasi Right-type or Slanted Tetrahedron*)**.** This tetrahedron has three right-angled triangular faces, with the right angles at different vertices, and the fourth one is acute, see face *ABC* in Fig. 1(c). On this face there are the second longest-edges of the tetrahedron. The longest-edge is a common hypotenuse of two right-angled triangular faces, see edge *OC* in Fig. 1(c).

The triangular face *ABC* in Fig. 1(c) can be equilateral, isosceles or scalene. For the first case, there will be three second longest-edges of the same length, where the edge *AB* is a hypotenuse. For the other two cases, there will be two different second-longest edges, with the edge *AB* the smaller of the two second longest-edges.

We call here new tetrahedron, the tetrahedron having two triangular faces of the right type and the other two are of obtuse type. The longest-edge is not a hypotenuse but the two different second longest-edges are, see Fig. 1(d). This tetrahedron will be denoted by T.

Definition 3 (*Similar Simplices*)**.** In general, any pair of simplices $T_1, T_2 \in \mathbb{R}^n$ are called *similar* if there exists a translation vector $\mathbf{a} \in \mathbb{R}^n$, a scaling factor $c > 0$, and an orthogonal matrix $\mathbf{Q} \in \mathbb{R}^{n\times n}$ such that $T_2 = \mathbf{a} + c\mathbf{Q}T_1$ [13].

The similarity class of a simplex does not depend on its vertex ordering.

Definition 4 (*Skeleton*)**.** Let τ be an n-simplicial mesh. The set $skt(\tau) = \{f : f \text{ is an } (n-1)\text{-face of any } T_i, \text{ with } T_i \in \tau\}$ will be called $(n-1)$-skeleton of τ, and it is also denoted by $(n-1)$-$skt(\tau)$. For instance, the skeleton of a triangulation in three dimensions are the triangular faces of the tetrahedra, and in two dimensions the skeleton is the set of the edges of the triangles.

Definition 5 (*The 4-triangle Longest-edge (4T-LE) Partition*)**.** The 4T-LE partition of a general triangle t_1, is obtained by performing first the longest-edge bisection of t_1, generating two subtriangles t' and t'', see Fig. 2(a). Then, these subtriangles are bisected by their common edge with original triangle t_1, see Fig. 2(b).

3. The 8T-LE partition applied to trirectangular tetrahedra

For any tetrahedron T, the *8-Tetrahedra Longest-Edge partition (8T-LE)* of T, produces 8 sub-tetrahedra by performing the 4T-LE partition of the faces of T, and then subdividing the interior of T consistently with the division of the faces. To perform this partition, the tetrahedron has to be previously classified in three types, according to the relative positions of its longest-edges [14–16].

Fig. 3 shows an example of the 8T-LE partition applied to an arbitrary tetrahedron, with vertices *A*, *B*, *C* and *D*, in which the longest-edge is *AB*, while edges *CD* and *AD* are the second longest-edges. According to the pseudocode in Section 3, the tetrahedron is classified type 3. In this article, we will study the similarity classes generated by 8T-LE partition when it is applied to a trirectangular tetrahedron, using simple geometrical arguments. The regular case has been studied in [5], where it has been proved that the 8T-LE partition only generates 4 similarity classes. Now we focus on the isosceles and scalene cases.

Let us label the longest-edge with number 1 and the opposite edge with number 6, see Figs. 3 and 4. The classification of the tetrahedron can be summarized as follows [14]:

Procedure Classification
/*Input variables: T tetrahedron

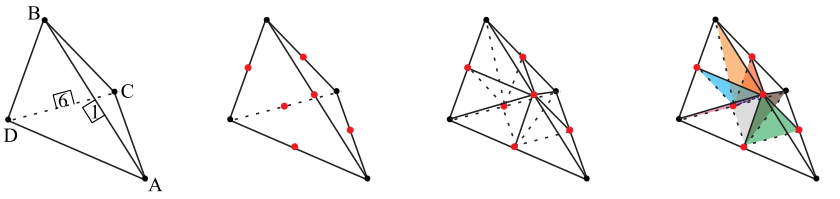

a) Initial tetrahedron b) Edge Subdivision c) Skeleton Subdivision d) Interior Subdivision

Fig. 3. 8T-LE partition of type 3 tetrahedron [*ABCD*].

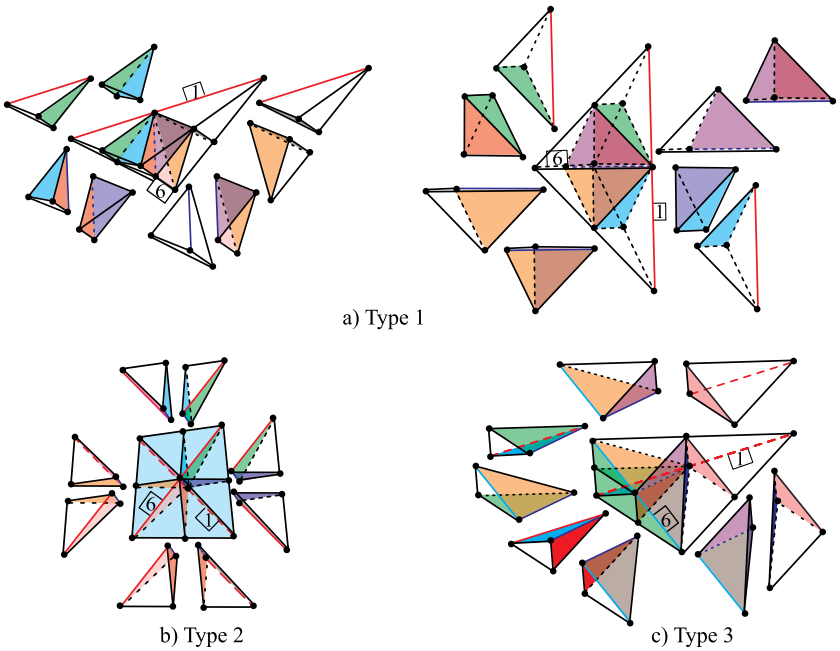

a) Type 1

b) Type 2 c) Type 3

Fig. 4. Classification of tetrahedra and the four refinement patterns for the 8T-LE partition.

Output variables: type */
If edge 6 is not the longest of any triangular face **then**
T is type 1
Else edge 6 is the longest of the two triangular faces sharing it **then**
T is type 2 (in blue colour in Fig. 4 b))
Else
T is type 3 (in green colour in Fig. 4 c))
End If

For the sake of clarity of exposition, we show in Fig. 4 the four refinement patterns (see [4,14–17]) associated to the three types of tetrahedra. The subtetrahedra generated have been depicted around its *"parents"*. Type 1 is associated with two patterns.

From now and on, we will study and analyze the isosceles and scalene cases for the trirectangular tetrahedron.

3.1. Isosceles trirectangular tetrahedron

In this case, there are two legs of equal length but different to the other one. This tetrahedron is classified type 1 by the 8T-LE partition.

A particular case for an isosceles trirectangular tetrahedron belonging to the Sommerville's tetrahedra family, is the well-known Sommerville tetrahedron number 2, ST_2, which can be obtained by dividing the Sommerville tetrahedron number 1, ST_1, into two similar tetrahedra ST_2, by a plane through the longest edge and the midpoint of the opposite edge [18]. Since the Sommerville tetrahedra are based on a particular splitting of the unit cube [19], tetrahedron ST_2 can also be obtained by bisecting the ST_1 tetrahedron by the cube face (see Fig. 5(a)), and the ST_1 tetrahedron is found by

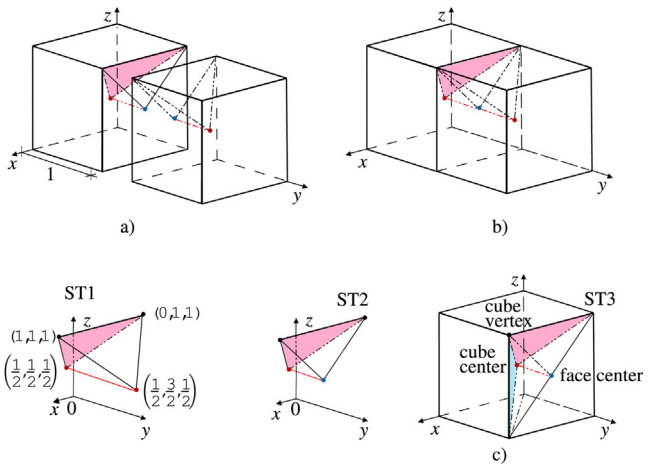

Fig. 5. Sommerville's tetrahedra family [19].

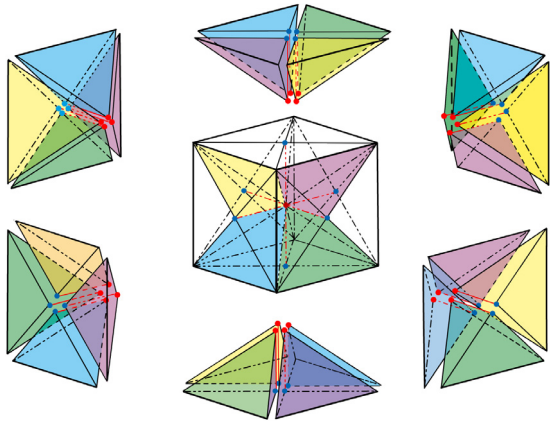

Fig. 6. Face-Centered 24-fold subdivision. The 24 tetrahedra ST2 are depicted around the cube in groups of four.

joining two vertices of the cube which share a common edge to the centers of two adjacent cubes, as it is shown in Fig. 5(b). Finally, the Sommerville tetrahedron number 3, ST_3, is obtained by from the ST_2 by joining two tetrahedra along a common face through a cube vertex, face center and cube center, see Fig. 5(c).

The ST_2 tetrahedron also appears when the Face Centered subdivision is carried out in the unit cube [7], generating 14, 16, 18, 20, 22 and 24 subtetrahedra ST_2, depending on the number of the face-centers added. Previously, the Face Divided subdivision of the unit cube is done in which 12 ST_3 Sommerville tetrahedra are generated from pyramids whose bases are the faces of the cube. Connecting each cube vertex to the body center, six square pyramids are obtained. Each of these pyramids are divided into two tetrahedra by an arbitrary face diagonal. This subdivision can be further subdivided by adding new vertices in the center of faces of the cube –which is equivalent to generate the second diagonal of the face–, generating the Face Centered subdivision. Adding some or all the face-centers gives subdivisions with 14, 16, 18, 20, 22 or 24 subtetrahedra, respectively, see Fig. 6. All these tetrahedra are ST_2.

Without loss of generality, the isosceles trirectangular tetrahedron to be studied has the vertices $A = (0, 0, 0)$, $B = (a, 0, 0)$, $C = (a, 0, b)$ and $D = (a, b, 0)$ with $b > a > 0$, see Fig. 7. This figure shows the subtetrahedra generated by the 8T-LE partition. Four subtetrahedra are similar to their father, and the remaining four subtetrahedra are two quasi right-type tetrahedra similar to each other -[*BEGH*] and [*BEFH*]-, and two new tetrahedra *T* -[*AEGH*] and [*AEFH*]-, which are also similar to one another. This congruency is shown by a mirror reflection by plane π_1, see top left corner of Fig. 8.

The subtetrahedra quasi right-type and the new one, called *T*, will be studied by the 8T-LE partition. For the quasi right-type subtetrahedron, edge *EH* is a common hypotenuse, and the two second longest-edges are on an isosceles triangular face with vertices *B*, *E* and *G*, with edges *BG* (which is a hypotenuse) and *EG* of the same length. Edge *BE* is the largest of all them, see Definition 2 and Figs. 7 and 8. The new classes of similarity for these subtetrahedra are depicted in Fig. 8.

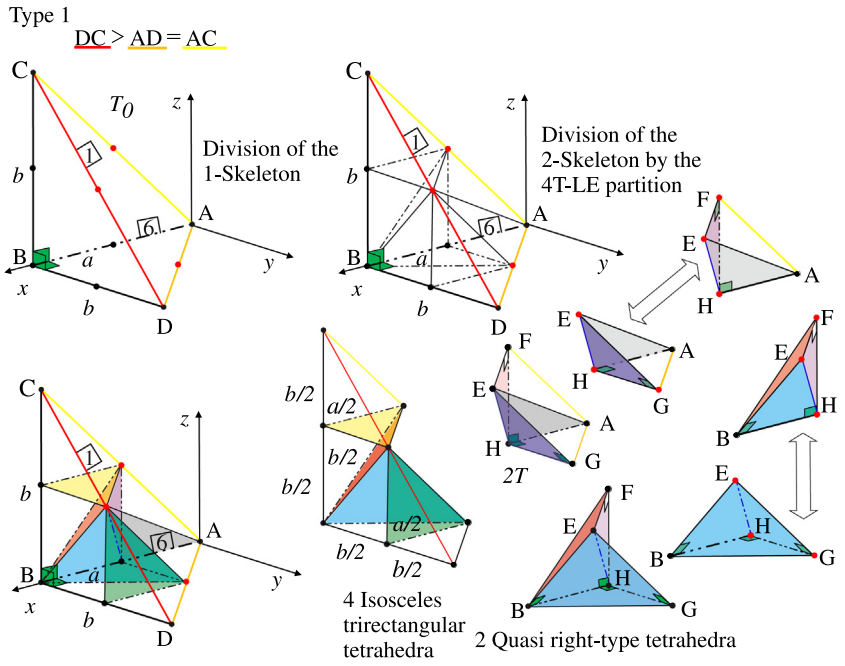

Fig. 7. 8T-LE partition applied to an isosceles trirectangular tetrahedron.

According to Figs. 8 and 9 we can see that:

- Cases (a), (f) and (h) are similar between them by Theorem 3, $T_3 \equiv T$.
- The other cases from (f) and (h) -tetrahedron T'-, are also similar to each other according to Theorem 3, $T_4 \equiv T'$.
- Case (b) is similar to the original tetrahedron T_0.
- Case (d) is similar to its father and also to the case (e). To prove this, both subsubtetrahedra are similar to each other by means of two consecutive mirror reflection through planes π_9 and π_{10} applied to the subsubtetrahedron marked with a diamond, as we can see on the bottom of Fig. 9.
- Cases (g) and (c) are similar between them, as we can see on the bottom of Fig. 9, according to three mirror reflection by planes π_9, π_{10} and π_{11} applied to the subsubtetrahedron marked with two diamonds, and also, similar to the quasi right-type subtetrahedron generated in the first generation with vertices B, E, G and H.

At this point, the last step is to check the two isosceles right-type subsubtetrahedra. According to [4], the 8T-LE partition applied to $T = T\,(a/4, b/4, b/4)$ tetrahedron generates four $T = T\,(a/8, b/8, b/8)$ tetrahedra similar to the original one, and two $T' = T'\,(b/8, a/8, b/8)$ tetrahedra, and applying this partition to the $T' = T'\,(b/4, a/4, b/4)$ tetrahedron, generates four $T = T\,(a/8, b/8, b/8)$ tetrahedra and four $T' = T'\,(b/8, a/8, b/8)$ tetrahedra similar to the original one. These tetrahedra will be called as T_3 and T_4, respectively.

Finally, the number of different classes of similarity is 5. Fig. 10 shows the relations between the different classes of similarity.

Let us denote by $T_i^{(n)}$ the number of tetrahedra of class T_i, after n iterative applications of the 8T-LE partition, to an initial isosceles trirectangular tetrahedron T_0. The recurrence relations associated to the 8T-LE partition of an initial isosceles trirectangular tetrahedron T_0, with initial conditions $T_0^{(0)} = 1$, $T_1^{(0)} = T_2^{(0)} = T_3^{(0)} = T_4^{(0)} = 0$, and also $T_3^{(1)} = T_4^{(1)} = 0$, are:

$$\left\{\begin{array}{l} T_0^{(n)} = 4T_0^{(n-1)} + 2T_2^{(n-1)} \\ T_1^{(n)} = 2T_0^{(n-1)} + 2T_1^{(n-1)} + 2T_2^{(n-1)} \\ T_2^{(n)} = 2T_0^{(n-1)} + 2T_1^{(n-1)} + 2T_2^{(n-1)} \\ T_3^{(n)} = 2T_1^{(n-1)} + 2T_2^{(n-1)} + 6T_3^{(n-1)} + 4T_4^{(n-1)} \\ T_4^{(n)} = 2T_1^{(n-1)} + 2T_3^{(n-1)} + 4T_4^{(n-1)} \end{array}\right\} \text{ for } n \geqslant 1. \tag{1}$$

Theorem 4. *Let T_0 be an isosceles trirectangular tetrahedron. Then,* $T_0^{(n)} = \dfrac{2^n(1+3^n)}{2}$, $T_1^{(n)} = T_2^{(n)} = \dfrac{2^n(3^n-1)}{2}$, $T_3^{(n)} = \dfrac{2^{3n+1} + 2^n(1-3^{n+1})}{3}$ $T_4^{(n)} = \dfrac{8^n + 2^{n-1}(1-3^{n+1})}{3}$.

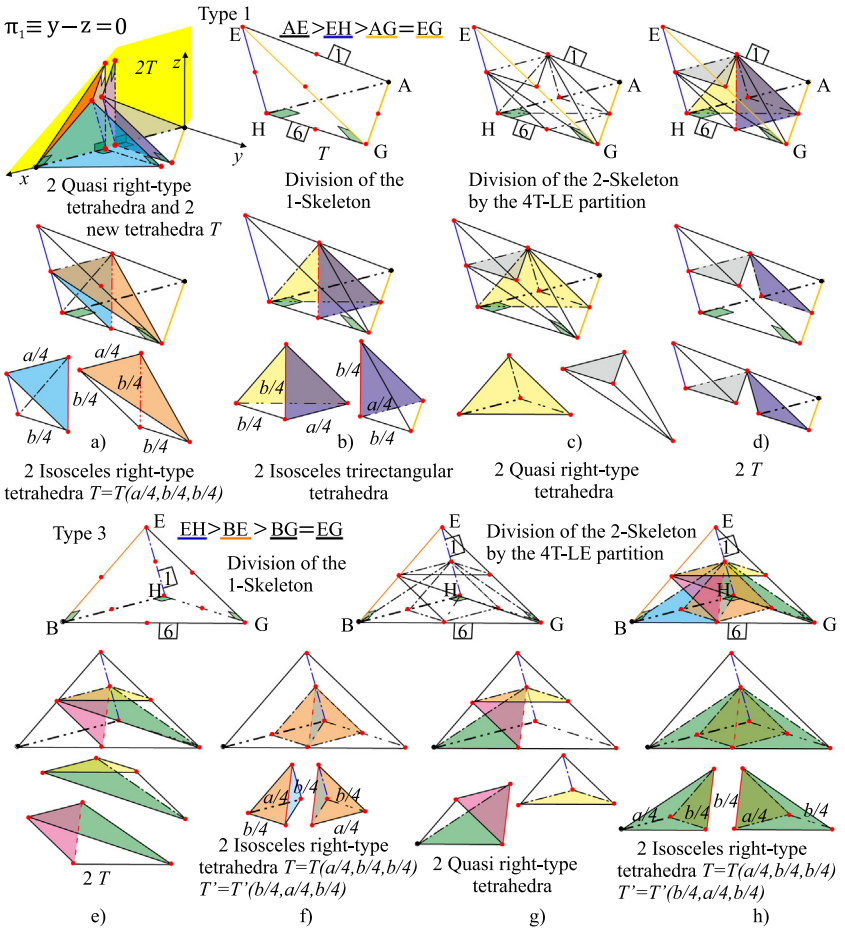

Fig. 8. 8T-LE partition applied to new subtetrahedron [*AEGH*] and quasi right-type subtetrahedron [*BEGH*], and similarity classes.

Proof. By induction. As a matter of an example, we will prove the last two formulas, $T_3^{(n)}$ and $T_4^{(n)}$. The formula given by the theorem is trivially true for $n = 0$ since $T_0^{(0)} = 1$. Let us suppose that the statement is true for $n = k - 1$, then $T_0^{(k-1)} = \frac{2^{k-1}(3^{k-1}+1)}{2}$, $T_1^{(k-1)} = T_2^{(k-1)} = \frac{2^{k-1}(3^{k-1}-1)}{2}$, $T_3^{(k-1)} = \frac{2^{3k-2}+2^{k-1}(1-3^k)}{3}$, $T_4^{(k-1)} = \frac{8^{k-1}+2^{k-2}(1-3^k)}{3}$. By Eqs. (1) we have,

$$T_3^{(k)} = 2T_1^{(k-1)} + 2T_2^{(k-1)} + 6T_3^{(k-1)} + 4T_4^{(k-1)} =$$

$$4\frac{2^{k-1}(3^{k-1}-1)}{2} + 6\frac{2^{3k-2}+2^{k-1}(1-3^k)}{3} + 4\frac{8^{k-1}+2^{k-2}(1-3^k)}{3} =$$

$$\frac{2^{3k+1}+2^k(1-3^{k+1})}{3}$$

$$T_4^{(k)} = 2T_1^{(k-1)} + 2T_3^{(k-1)} + 4T_4^{(k-1)} =$$

$$2\frac{2^{k-1}(3^{k-1}-1)}{2} + 2\frac{2^{3k-2}+2^{k-1}(1-3^k)}{3} + 4\frac{8^{k-1}+2^{k-2}(1-3^k)}{3} =$$

$$\frac{8^k+2^{k-1}(1-3^{k+1})}{3}. \quad \square$$

According to [20], let s_n be the number of different tetrahedra similarity classes that have been generated during the first n steps by the 8T-LE partition applied to a single tetrahedron.

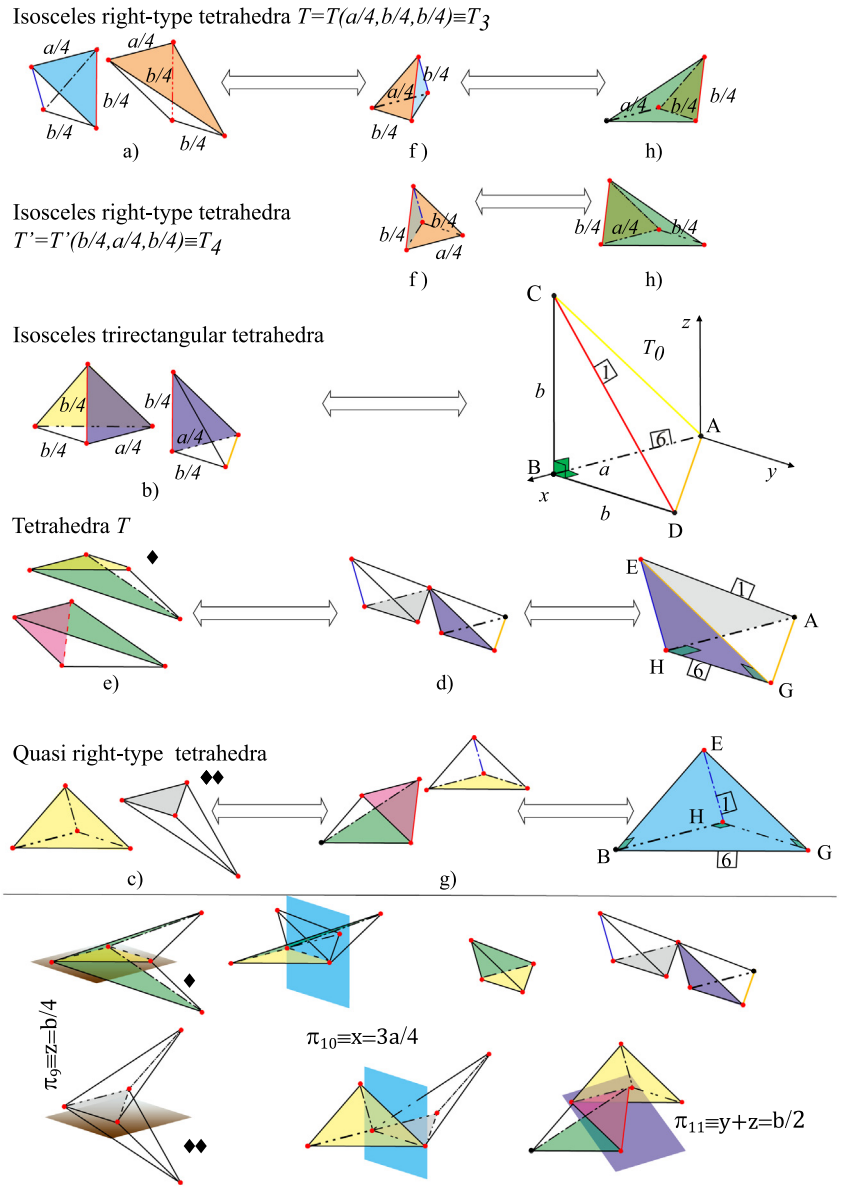

Fig. 9. Study of similarity classes. Subtetrahedra [*AEGH*] and [*BEGH*] from the first and second generation are similar.

The sequence $\{s_n\}_{n=0}^{\infty}$, where $s_0 = 1$, is non decreasing. In many cases we get $s_n < s_{n+1}$ for all n, but sometimes there is an integer $n_0 > 0$ such that

$$s_n = s_{n+1} \quad \forall n \geqslant n_0. \tag{2}$$

For this case we have, $s_0 = 1$, $s_1 = 3$, $s_2 = 5$ and the whole sequence s_n is $1, 3, 5, 5, 5, \ldots$ and $n_0 = 3$.

When the 8T-LE partition is applied to an isosceles trirectangular tetrahedron –which is a nonobtuse tetrahedron–, there appear two obtuse tetrahedra T_1 and T_2. However, Fig. 11 shows that each triangulation is less obtuse than the previous one, and the evolution of the percentage of the volume covered by the by both isosceles right-type tetrahedra, T_3 and T_4, are much greater in every step of refinement compared to the other classes of tetrahedra. The total number of tetrahedra generated at stage 8 is 16, 777, 216.

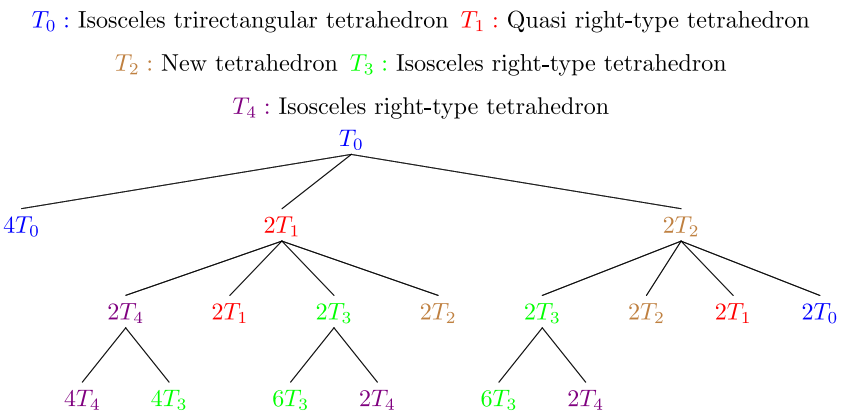

Fig. 10. Genealogy tree of the similarity classes for the isosceles trirectangular tetrahedron.

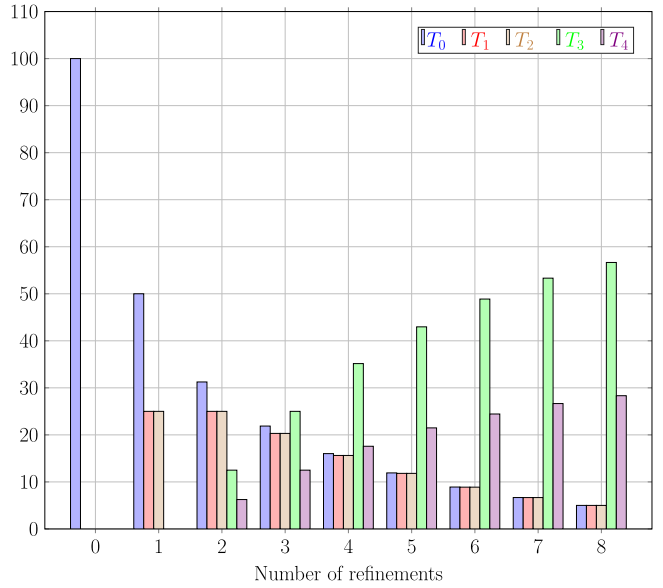

Fig. 11. Percentage of volume of each similarity class as the number of refinements grows.

The percentage covered by each class of right-type tetrahedra is shown more clearly solving the limit when n tends to infinity of these expressions, $\lim_{n\to\infty} \dfrac{T_3^{(n)}}{\sum_{i=0}^{4} T_i^{(n)}}$ and $\lim_{n\to\infty} \dfrac{T_4^{(n)}}{\sum_{i=0}^{4} T_i^{(n)}}$. For the first one,

$$\lim_{n\to\infty} \frac{T_3^{(n)}}{T_0^{(n)} + T_1^{(n)} + T_2^{(n)} + T_3^{(n)} + T_4^{(n)}} =$$

$$\lim_{n\to\infty} \frac{\dfrac{2^{3n+1} + 2^n(1-3^{n+1})}{3}}{\dfrac{2^n(1+3^n)}{2} + 2\dfrac{2^n(3^n-1)}{2} + \dfrac{2^{3n+1} + 2^n(1-3^{n+1})}{3} + \dfrac{8^n + 2^{n-1}(1-3^{n+1})}{3}}$$

$$= \lim_{n\to\infty} \frac{2^{3n+1} + 2^n(1-3^{n+1})}{2^{3n}3} = \frac{2}{3}.$$

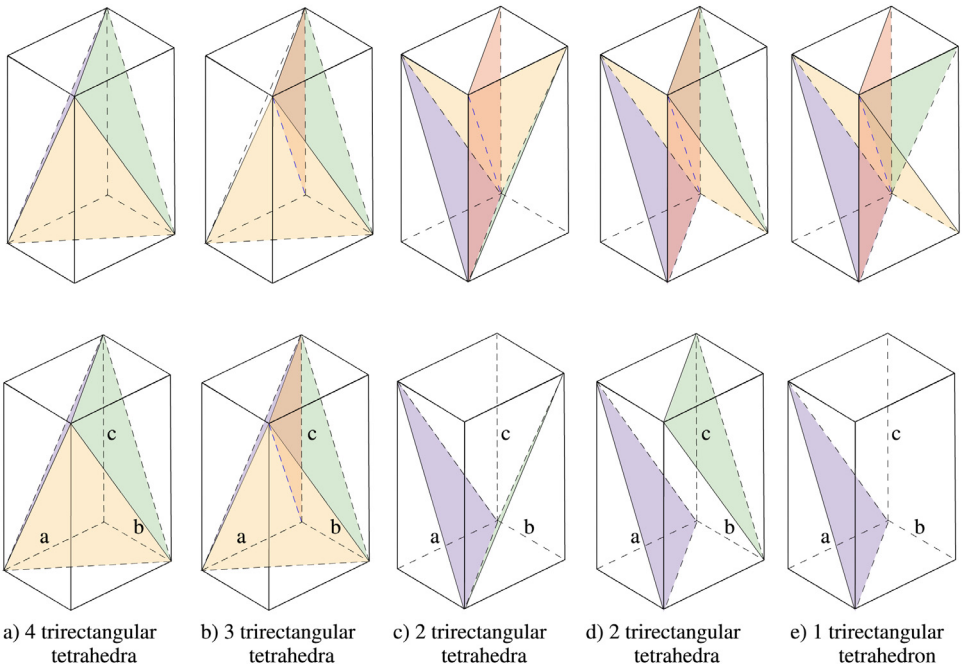

Fig. 12. An example of a triangulation of an hexahedron.

Evaluating the limit for the second expression,

$$\lim_{n\to\infty} \frac{T_4^{(n)}}{T_0^{(n)} + T_1^{(n)} + T_2^{(n)} + T_3^{(n)} + T_4^{(n)}} =$$

$$\lim_{n\to\infty} \frac{\dfrac{8^n + 2^{n-1}(1-3^{n+1})}{3}}{\dfrac{2^n(1+3^n)}{2} + 2\dfrac{2^n(3^n-1)}{2} + \dfrac{2^{3n+1} + 2^n(1-3^{n+1})}{3} + \dfrac{8^n + 2^{n-1}(1-3^{n+1})}{3}}$$

$$= \lim_{n\to\infty} \frac{8^n + 2^{n-1}(1-3^{n+1})}{2^{3n}3} = \frac{1}{3}.$$

According to the results of those limits, the percentage of volume covered by the T_3 isosceles right-type will be $66.\overline{6}\%$, and for the other isosceles right-type tetrahedron T_4, will be $33.\overline{3}\%$.

3.2. Scalene trirectangular tetrahedron

It should be noted that when a hexahedral mesh is converted in a tetrahedral mesh, many trirectangular tetrahedra appear. Fig. 12 shows an example of a triangulation of a hexahedron into five and six tetrahedra respectively, in which a scalene trirectangular tetrahedron is involved.

In this case, $a \neq b \neq c$. For this purpose we focus on a general tetrahedron shown in Fig. 13(a) with vertices $O = (0, 0, 0)$, $A = (a, 0, 0)$, $B = (0, b, 0)$ and $C = (0, 0, c)$ with $b > c > a$ and $a > 0$. This tetrahedron is type 1.

Fig. 13 shows that four subtetrahedra are similar to the original one. The remaining four subtetrahedra generated are all of them different. There are two different quasi right-type subtetrahedra, T_1 and T_3, and two different new subtetrahedra, T_2 and T_4. Subtetrahedra T_1 and T_3 are classified type 3 by the 8T-LE partition, and T_2 and T_4 subtetrahedra are classified type 1 by the same partition. All these subtetrahedra have the vertices locally labeled with numbers from 1 to 4. For the quasi right-type subtetrahedra (T_1 and T_3), the two second longest-edges are on a scalene triangular face, where the smaller one is a hypotenuse of the other face sharing it. Below we will study each one of these tetrahedra.

3.2.1. Subtetrahedron T_1

Fig. 14 shows the different classes of tetrahedra generated when the 8T-LE partition is applied to a subtetrahedron T_1.

There are two scalene right-type subsubtetrahedra T_{r_1} and two scalene right-type subsubtetrahedra T_{r_2}. According to [4], the 8T-LE partition applied to each subsubtetrahedron T_{r_1} generates 4 T_{r_1}, 2 T_{r_2} and 2 T_{r_3}, and for the second scalene right-type subsubtetrahedron, the classes generated are 4 T_{r_2}, 2 T_{r_1} and 2 T_{r_3}. Finally, for the T_{r_3} scalene right-type

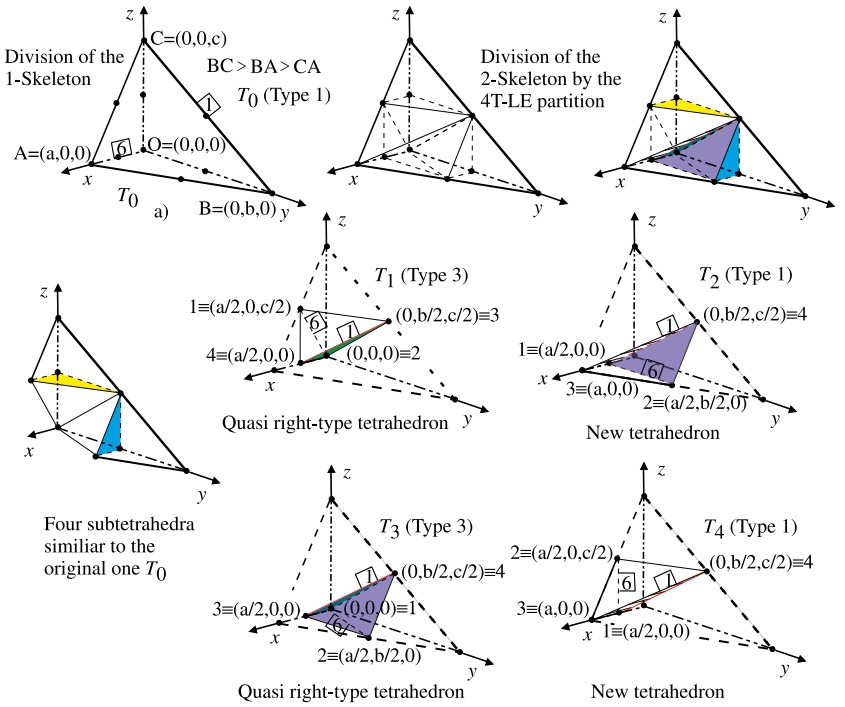

Fig. 13. Division of a general scalene tetrahedron by the 8T-LE partition.

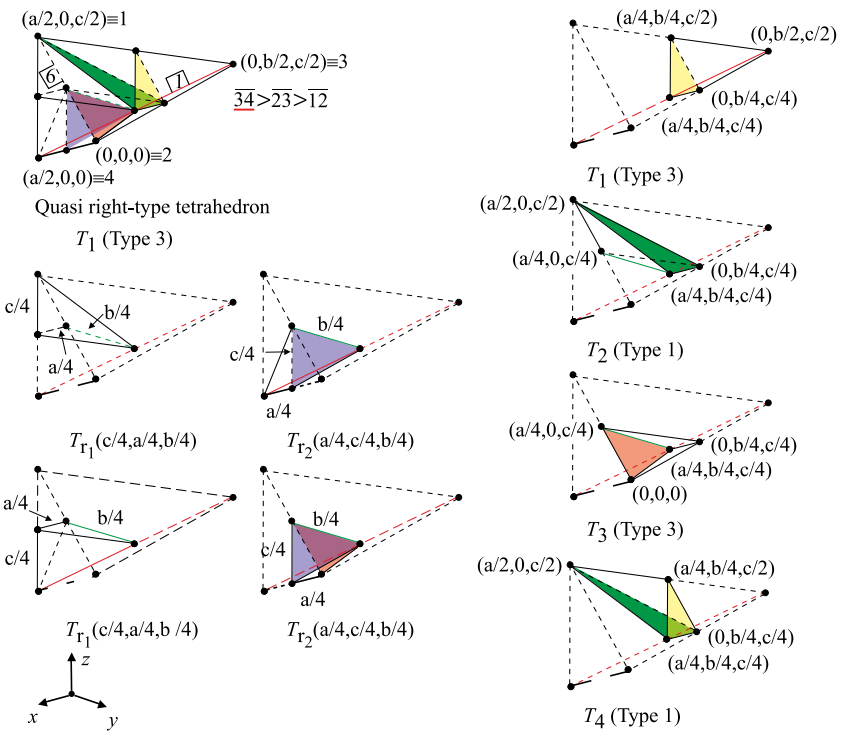

Fig. 14. 8T-LE partition applied to subtetrahedron T_1 and similarity classes.

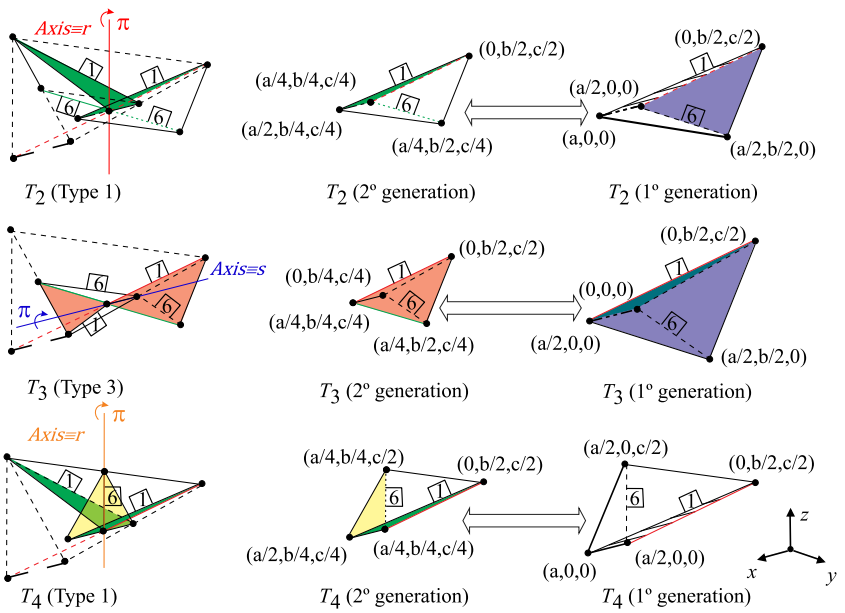

Fig. 15. Study of subsubtetrahedra T_2, T_3 and T_4.

subsubtetrahedron –which will appear later–, there are 4 T_{r_3}, 2 T_{r_1} and 2 T_{r_2}. In the right top corner of the figure, it is shown that only one subsubtetrahedron is similar to subtetrahedron T_1. So the next step is to study if for the three remaining subsubtetrahedra called as T_2, T_3 and T_4 belong to those classes, shown in Fig. 13.

Fig. 15 illustrates that by means of two different π clockwise rotations around axes $r \equiv (a/4, b/4, c/4) + t(0, 0, c/4)$ and $s \equiv (a/4, b/4, c/4) + \lambda(a/4, 0, 0)$, respectively applied to subsubtetrahedra T_2 and T_4, and to subsubtetrahedron T_3, those subtetrahedra T_2, T_3 and T_4 from the first generation and depicted in Fig. 13, and the respective subsubtetrahedra from the second generation, belong to the same similarity classes.

3.2.2. Subtetrahedron T_2

We will use Fig. 16. The top right corner of the figure shows that two subsubtetrahedra are similar to subtetrahedron T_2, two subsubtetrahedra are similar to the original T_0, another two are scalene right-type subsubtetrahedra T_{r_2}, and finally, two subsubtetrahedra are class T_3.

It is clear that the subsubtetrahedron with vertices A_4, B_4, C_4 and D_4 is similar to the subtetrahedron T_3 from the first generation sketched in Fig. 13. Moreover, subsubtetrahedron with vertices A_1, B_1, C_1 and D_1, is similar to subsubtetrahedron with vertices A_4, B_4, C_4 and D_4, and hence, it is similar to first subtetrahedron T_3. To prove this similarity, we use two π rotations around axis s and axis r, respectively, counterclockwise and clockwise, see Fig. 16.

3.2.3. Subtetrahedron T_3

Fig. 17 shows the different classes of similarity generated when the 8T-LE partition is applied to this tetrahedron. There is only one descendant similar to subtetrahedron T_3, located in the right top corner of the previous figure, and two scalene right-type subsubtetrahedra, T_{r_1} and T_{r_3}, respectively, which have already been studied.

For the remaining subsubtetrahedra T_1, T_2 and T_4, the procedure is exactly the same as for the subtetrahedron T_1. In Fig. 18, and according to the axes s -counterclockwise- and r -clockwise-, it is proved that the subsubtetrahedra T_1, T_2 and T_4 from the second generation, belong to the same class that the respective T_1, T_2 and T_4, from the first generation, drawn in Fig. 13.

3.2.4. Subtetrahedron T_4

Fig. 19 shows the different classes of similarity generated. The top right corner shows that two subsubtetrahedra are similar to subtetrahedron T_4, two subsubtetrahedra are similar to the original T_0 and other two subsubtetrahedra are scalene right-type subsubtetrahedra, T_{r_3}. Through a π clockwise rotation around axis r applied to one of the subsubtetrahedra generated with vertices A_3, B_3, C_3 and D_3, this tetrahedron is similar to the other subsubtetrahedron with vertices A_2, B_2, C_2 and D_2. In addition, both subsubtetrahedra are also similar to subtetrahedron T_1 from the first generation depicted in Fig. 13.

To clarify the results obtained, the next genealogy tree is used in order to show the number of classes of similarity generated when the 8T-LE partition is applied to the scalene trirectangular tetrahedron, see Fig. 20. Each class of similarity

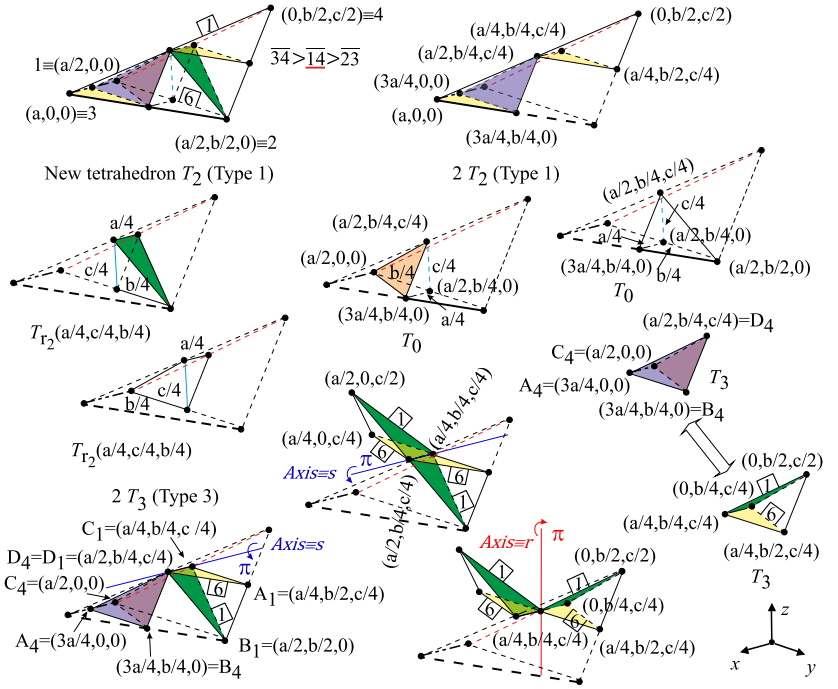

Fig. 16. 8T-LE partition applied to subtetrahedron T_2 and study of classes of similarity.

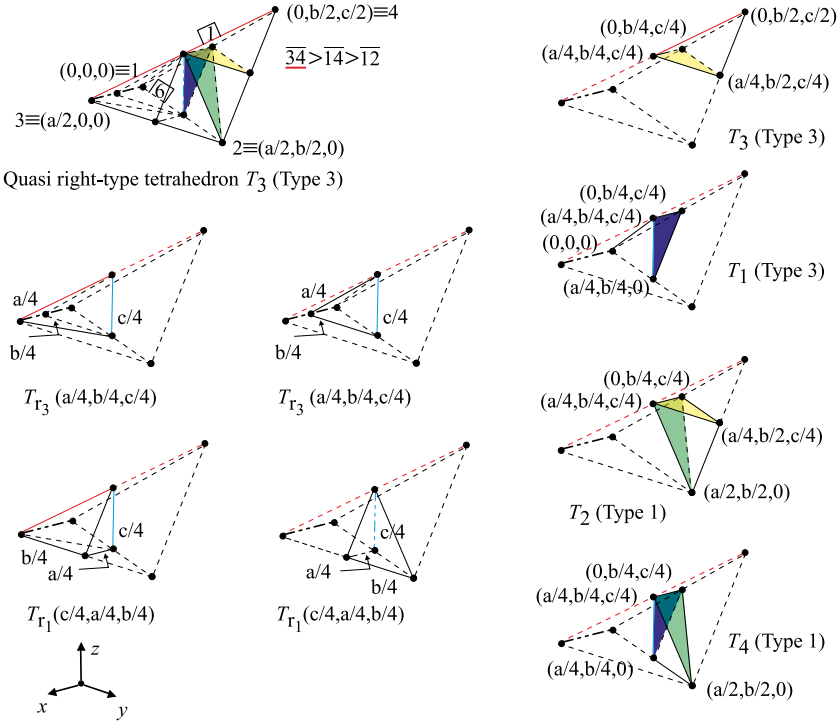

Fig. 17. 8T-LE partition applied to subtetrahedron T_3 and similarity classes.

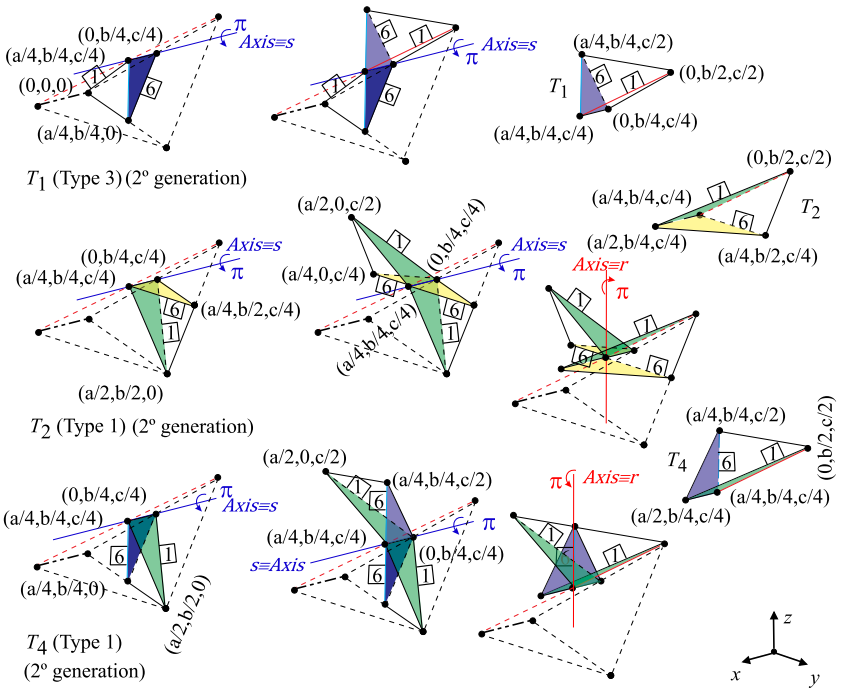

Fig. 18. Study of subsubtetrahedra T_1, T_2 and T_4.

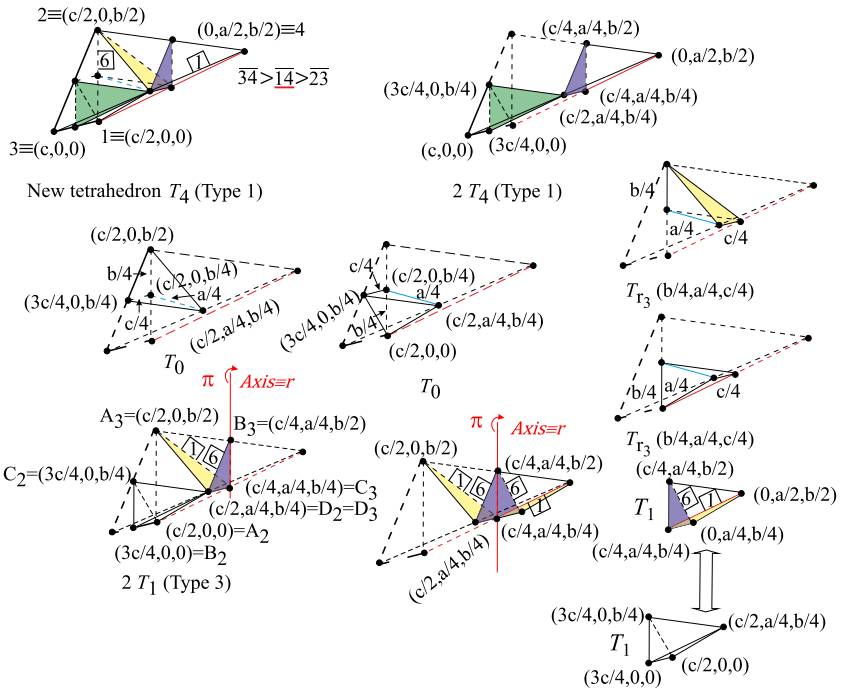

Fig. 19. 8T-LE partition applied to subtetrahedron T_4 and study of classes of similarity.

has been described by color and name. The number of different classes of similarity is 8 and the total amount of tetrahedra in the last refinement step is 8^8.

Let us denote by $T_i^{(n)}$ the number of tetrahedra of class T_i, with $r_1 \equiv 5$, $r_2 \equiv 6$ and $r_3 \equiv 7$, after n iterative applications of the 8T-LE partition to an initial scalene trirectangular tetrahedron T_0. The recurrence relations associated to the 8T-LE

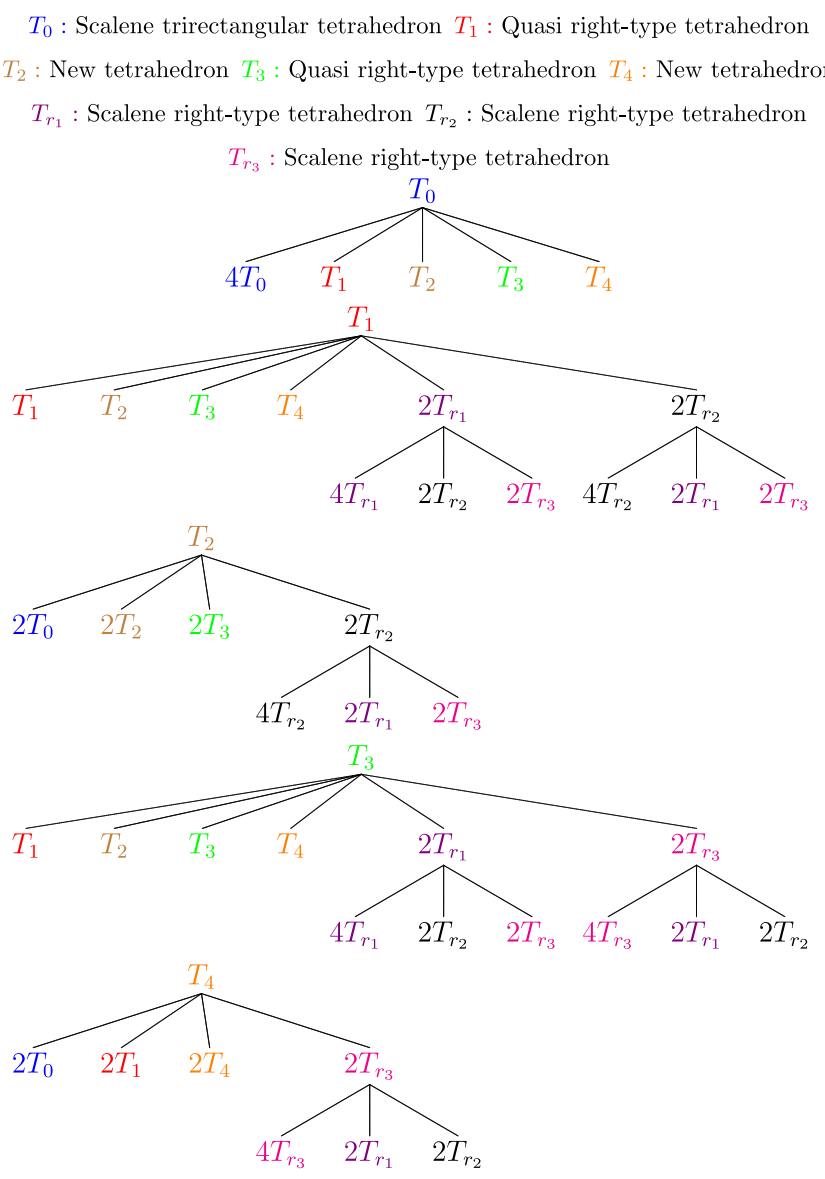

Fig. 20. Genealogy tree of the different classes of similarity for the scalene trirectangular tetrahedron.

partition of an initial scalene trirectangular tetrahedron T_0, with initial conditions $T_0^{(0)} = 1$, $T_1^{(0)} = T_2^{(0)} = T_3^{(0)} = T_4^{(0)} = T_{r_1}^{(0)} = T_{r_2}^{(0)} = T_{r_3}^{(0)} = 0$, and also $T_{r_1}^{(1)} = T_{r_2}^{(1)} = T_{r_3}^{(1)} = 0$, are:

$$\left\{\begin{array}{l} T_0^{(n)} = 4T_0^{(n-1)} + 2T_2^{(n-1)} + 2T_4^{(n-1)} \\ T_1^{(n)} = T_0^{(n-1)} + T_1^{(n-1)} + T_3^{(n-1)} + 2T_4^{(n-1)} \\ T_2^{(n)} = T_0^{(n-1)} + T_1^{(n-1)} + 2T_2^{(n-1)} + T_3^{(n-1)} \\ T_3^{(n)} = T_0^{(n-1)} + T_1^{(n-1)} + 2T_2^{(n-1)} + T_3^{(n-1)} \\ T_4^{(n)} = T_0^{(n-1)} + T_1^{(n-1)} + T_3^{(n-1)} + 2T_4^{(n-1)} \\ T_{r_1}^{(n)} = 2T_1^{(n-1)} + 2T_3^{(n-1)} + 4T_{r_1}^{(n-1)} + 2T_{r_2}^{(n-1)} + 2T_{r_3}^{(n-1)} \\ T_{r_2}^{(n)} = 2T_1^{(n-1)} + 2T_2^{(n-1)} + 2T_{r_1}^{(n-1)} + 4T_{r_2}^{(n-1)} + 2T_{r_3}^{(n-1)} \\ T_{r_3}^{(n)} = 2T_3^{(n-1)} + 2T_4^{(n-1)} + 2T_{r_1}^{(n-1)} + 2T_{r_2}^{(n-1)} + 4T_{r_3}^{(n-1)} \end{array}\right\} \text{ for } n \geqslant 1. \tag{3}$$

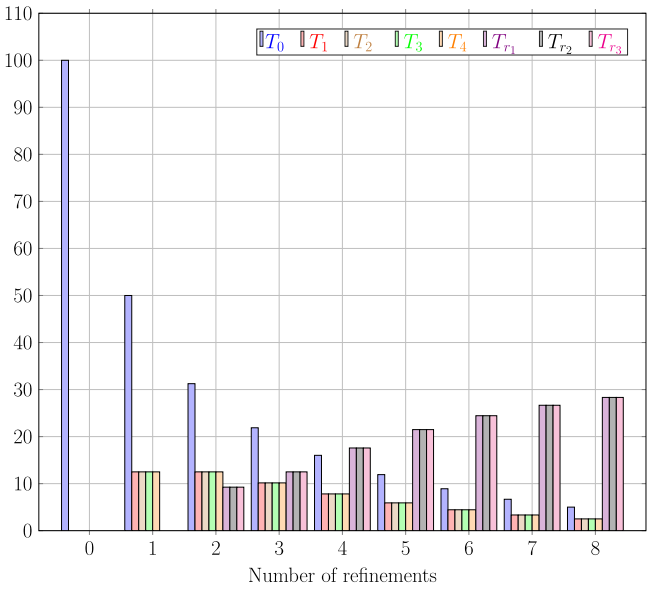

Fig. 21. Percentage of volume of each similarity class as the number of refinements grows.

Theorem 5. *Let T_0 be a scalene trirectangular tetrahedron. Then,* $T_0^{(n)} = \dfrac{2^n(1+3^n)}{2}$, $T_1^{(n)} = T_2^{(n)} = T_3^{(n)} = T_4^{(n)} = \dfrac{2^n(3^n-1)}{4}$, $T_{r_1}^{(n)} = T_{r_2}^{(n)} = T_{r_3}^{(n)} = \dfrac{2^{n-1}(1+2^{2n+1}-3^{n+1})}{3}$.

Proof. By induction in a similar way as in Theorem 4. □

For this example we have, $s_0 = 1$, $s_1 = 5$, $s_2 = 8$ and the whole sequence s_n is $1, 5, 8, 8, 8, \ldots$ and $n_0 = 5$.

According to Fig. 21, it is clear that asymptotically the scalene right-type tetrahedra will cover the entire volume. Each scalene right-type tetrahedron will cover $33.\overline{3}\%$, since the $\lim_{n\to\infty} \dfrac{T_5^{(n)}}{\sum_{i=0}^{7} T_i^{(n)}} = \dfrac{1}{3}$. We get the same result for the scalene right-type tetrahedra T_6 and T_7, and to prove one of them we just need to solve the limit.

$$\lim_{n\to\infty} \frac{T_5^{(n)}}{T_0^{(n)} + T_1^{(n)} + T_2^{(n)} + T_3^{(n)} + T_4^{(n)} + T_5^{(n)} + T_6^{(n)} + T_7^{(n)}} =$$

$$\lim_{n\to\infty} \frac{\dfrac{2^{n-1}(1+2^{2n+1}-3^{n+1})}{3}}{\dfrac{2^n(1+3^n)}{2} + 4\dfrac{2^n(3^n-1)}{4} + 3\dfrac{2^{n-1}(1+2^{2n+1}-3^{n+1})}{3}} =$$

$$\lim_{n\to\infty} \frac{1+2^{2n+1}-3^{n+1}}{3(1+3^n)+6(3^n-1)+3(1+2^{2n+1}-3^{n+1})} =$$

$$\lim_{n\to\infty} \left(\frac{1}{2^{2n+1}3} + \frac{2^{2n+1}}{2^{2n+1}3} - \frac{3^n}{2^{2n+1}} \right) = 0 + \frac{1}{3} - 0 = \frac{1}{3}.$$

4. Conclusions

We have studied the number of dissimilar classes generated when the 8T-LE partition is applied to a trirectangular tetrahedron.

1. The number of similarity classes generated by the 8T-LE partition when it is recurrently applied to a trirectangular tetrahedron are respectively, 4, 5 and 8, depending on if the tetrahedron is regular, isosceles or scalene. Therefore, in any case a finite number of similarity classes is obtained, so non-degeneracy and the stability of the triangulation follow straightforwardly.

2. The number of similarity classes is directly related to the total computational cost, because many data can be computed and stored only once per element of a given similarity class. Hence, from a computational point of view, the number of similarity classes should be as small as possible.
3. When the number of refinement grows, most of the tetrahedra generated are of the right-type. For the isosceles trirectangular tetrahedron, the two different isosceles right-type tetrahedra cover respectively $\frac{2}{3}$ and $\frac{1}{3}$ of the whole volume. While for the scalene trirectangular tetrahedron the three different scalene right-type tetrahedra cover each one $\frac{1}{3}$ of the volume.
4. Note that since the right-type tetrahedra are nonobtuse, the quality of the generated meshes improves at each step of refinement.

CRediT authorship contribution statement

Miguel A. Padrón: Conceptualization, Methodology, Investigation, Visualization, Writing – original draft, Validation, Supervision, Writing – review & editing. **Ángel Plaza:** Conceptualization, Methodology, Investigation, Visualization, Writing – original draft, Validation, Supervision, Writing – review and editing.

Acknowledgment

The authors were supported by the Project Puente Cabildo 2018-01 by the Cabildo de Las Palmas de Gran Canaria.

References

[1] M.C. Rivara, Algorithms for refining triangular grids suitable for adaptive and multigrid techniques, Internat. J. Numer. Methods Engrg. 20 (4) (1984) 745–756, http://dx.doi.org/10.1002/nme.1620200412.
[2] A. Plaza, J.P. Suárez, M.A. Padrón, S. Falcón, D. Amieiro, Mesh quality improvement and other properties in the four-triangles longest-edge partition, Comput. Aid. Geom. Desig. 21 (2004) 253–369, http://dx.doi.org/10.1016/j.cagd.2004.01.001.
[3] J.A.D. Loera, J. Rambau, F. Santos, Triangulations: Structures for algorithms and applications, in: Algorihtms and Computation in Mathematics, Vol. 25, Springer-Verlag Heidelberg, New York, 2010, http://dx.doi.org/10.1007/978-3-642-12971-1.
[4] A. Plaza, M.A. Padrón, J.P. Suárez, S. Falcón, The 8-tetrahedra longest-edge partition of right-type tetrahedra, Finit. Elem. Anal. Desig. 41 (3) (2004) 253–265, http://dx.doi.org/10.1016/j.finel.2004.04.005.
[5] M.A. Padrón, A. Plaza, The 8T-LE partition applied to the obtuse triangulations of the 3D-cube, Math. Comput. Simul. 176 (1) (2020) 254–265, http://dx.doi.org/10.1016/j.matcom.2020.01.011.
[6] J. Brandts, A. Cihangir, Enumeration and investigation of acute 0/1-simplices modulo the action of the hyperoctahedral group, Special Matrices 5 (1) (2017) 158–201, http://dx.doi.org/10.1515/spma-2017-0014.
[7] G. Albertelli, R.A. Crawfis, Efficient subdivision of finite element datasets into consistent tetrahedra, in: Proceedings Visualization 97, IEEE Computer Society Technical Committee on Computer Graphics, in Cooperation with ACM SIGGRAPH, Phoenix, AZ, United States, 1997, pp. 213–219.
[8] R. Schneiders, Octree-based hexahedral mesh generation, Int. J. Comput. Geom. Appl. 10 (4) (2000) 383–398, http://dx.doi.org/10.1142/S021819590000022X.
[9] S. Korotov, M. Křížek, Local nonobtuse tetrahedral refinements around an edge, Appl. Math. Comput. 219 (13) (2013) 7236–7240, http://dx.doi.org/10.1016/j.amc.2011.03.143.
[10] T. Todorov, The optimal refinement strategy for 3-D simplicial meshes, Comput. Math. Appl. 66 (2013) 1272–1283, http://dx.doi.org/10.1016/j.camwa.2013.07.026.
[11] M. Křížek, Superconvergence phenomena on three-dimensional elasticity, Int. J. Numer. Anal. Model. 2 (1) (2005) 43–56.
[12] J. Brandts, S. Korotov, M. Křížek, J. Šolc, On nonobtuse simplicial partitions, SIAM Rev. 51 (2) (2009) 317–335, http://dx.doi.org/10.1137/060669073.
[13] A. Plaza, The eight-tetrahedra longest-edge partition and kuhn triangulations, Comput. Math. Appl. 54 (2007) 427–433, http://dx.doi.org/10.1016/j.camwa.2007.01.023.
[14] A. Plaza, G.F. Carey, Refinement of simplicial grids based on the skeleton, Appl. Numer. Math. 32 (2) (2000) 195–218, http://dx.doi.org/10.1016/S0168-9274(99)00022-7.
[15] M.A. Padrón, J.P. Suárez, A. Plaza, A comparative study between some bisection based partitions in 3D, Appl. Numer. Math. 55 (4) (2005) 357–367, http://dx.doi.org/10.1016/j.apnum.2005.04.035.
[16] A. Plaza, M.A. Padrón, J.P. Suárez, Non-degeneracy study of the 8-tetrahedra longest-edge partition, Appl. Numer. Math. 55 (4) (2005) 458–472, http://dx.doi.org/10.1016/j.apnum.2004.12.003.
[17] A. Plaza, M.C. Rivara, Average adjacencies for tetrahedral skeleton-regular partitions, J. Comput. Appl. Math. 177 (1) (2005) 141–158, http://dx.doi.org/10.1016/j.cam.2004.09.013.
[18] D.M.Y. Sommerville, Space-filling tetrahedra in euclidean space, Proc. Edinb. Math. Soc. 41 (1923) 49–57, http://dx.doi.org/10.1017/S001309150007783X.
[19] M. Senechal, Which tetrahedra fill space? Math. Mag. 54 (5) (1981) 227–243, http://dx.doi.org/10.2307/2689983.
[20] A. Hannukainen, S. Korotov, M. Křížek, On numerical regularity of the face-to-face longest-edge bisection algorithm for tetrahedral partitions, Sci. Comput. Progr. 90 (2014) 34–41, http://dx.doi.org/10.1016/j.scico.2013.05.002.